Cell Cycle 14:17, 2785–2797; September 1, 2015; © 2015 Taylor & Francis Group, LLC

Predictive and comparative analysis of *Ebolavirus* proteins

Qian Cong[1], Jimin Pei[2], and Nick V Grishin[1,2,*]

[1]Departments of Biophysics and Biochemistry; University of Texas Southwestern Medical Center at Dallas; Dallas, TX USA; [2]Howard Hughes Medical Institute; University of Texas Southwestern Medical Center at Dallas; Dallas, TX USA

Keywords: comparative analysis, *Ebolavirus*, functional site prediction, Pathogenicity, structure prediction

Ebolavirus is the pathogen for Ebola Hemorrhagic Fever (EHF). This disease exhibits a high fatality rate and has recently reached a historically epidemic proportion in West Africa. Out of the 5 known *Ebolavirus* species, only *Reston ebolavirus* has lost human pathogenicity, while retaining the ability to cause EHF in long-tailed macaque. Significant efforts have been spent to determine the three-dimensional (3D) structures of *Ebolavirus* proteins, to study their interaction with host proteins, and to identify the functional motifs in these viral proteins. Here, in light of these experimental results, we apply computational analysis to predict the 3D structures and functional sites for *Ebolavirus* protein domains with unknown structure, including a zinc-finger domain of VP30, the RNA-dependent RNA polymerase catalytic domain and a methyltransferase domain of protein L. In addition, we compare sequences of proteins that interact with *Ebolavirus* proteins from RESTV-resistant primates with those from RESTV-susceptible monkeys. The host proteins that interact with GP and VP35 show an elevated level of sequence divergence between the RESTV-resistant and RESTV-susceptible species, suggesting that they may be responsible for host specificity. Meanwhile, we detect variable positions in protein sequences that are likely associated with the loss of human pathogenicity in RESTV, map them onto the 3D structures and compare their positions to known functional sites. VP35 and VP30 are significantly enriched in these potential pathogenicity determinants and the clustering of such positions on the surfaces of VP35 and GP suggests possible uncharacterized interaction sites with host proteins that contribute to the virulence of *Ebolavirus*.

Introduction

Zaire Ebolavirus, the pathogen for Ebola Hemorrhagic Fever (EHF) with a 25–90% fatality rate,[1] continues to threaten people's lives. The current (2013 – Jun. 2015) West African outbreak of EHF has infected more than 27,000 people and caused 11,000 deaths.[2] The genus *Ebolavirus* contains 5 known species: *Bundibugyo* (BDBV), *Reston* (RESTV), *Sudan* (SUDV), *Taï Forest* (TAFV) and *Zaire ebolavirus* (ZEBOV).[3] The current outbreak is associated with ZEBOV.[4] Four *Ebolavirus* species cause EHF in human, with the sole exception being RESTV.[5] RESTV can cause EHF to long-tailed macaque (*Macaca fascicularis*). People who had contact with RESTV-infected monkeys tested positive for RESTV antibodies but did not develop symptoms associated with EHF.[5]

Ebolavirus belongs to the order *Mononegavirales* and the family *Filoviridae*.[3] Its RNA genome encodes the following 7 protein products: Envelope glycoprotein (GP), Nucleoprotein (NP), RNA-dependent RNA polymerase L (L), Membrane-associated protein VP24 (VP24), Minor nucleoprotein VP30 (VP30), Polymerase cofactor VP35 (VP35), and Matrix protein VP40 (VP40). The GP transcript can be edited,[6] and the gene product can be processed by host protease, giving rise to 4 alternative forms of gene products: GP1,2; GP1,2delta; sGP and ssGP. Host furin can cleave the longest product translated from edited GP mRNA and generate GP1,2, which consists of 2 peptide chains connected by a disulfide bond,[7,8] GP1 and GP2. GP1,2 is assembled on the membrane of *Ebolavirus* and mediates cell entry. GP1,2delta is the processed product after removal of the C-terminal transmembrane region of GP1,2 by host ADAM17.[9] Other products of the GP gene, sGP and ssGP are translated from the unedited mRNA and alternatively edited mRNA, respectively.[10,11] These products share the N-terminal 295 residues with GP1,2, but differ in their short tails (69 and 3 residues, respectively). GP1,2delta, sGP and ssGP may prevent the neutralizing antibodies from binding GP1,2 on the virus surface, contributing to the immune evasion of the virus.[12]

In addition to serving as structural components, the *Ebolavirus* proteins play multiple roles in the virus life cycle. GP mediates cell entry[13,14] and membrane fusion[15,16] between the virus and the host cell. NP encapsidates the genome and protects it from nucleases.[17,18] VP30 is a transcription anti-terminator[19,20] and regulates the switch between transcription and replication.[21,22] VP35 acts as a cofactor of the polymerase,[23,24] and VP40 may also play a role in genome replication and transcription.[25] VP24 and VP35 participate in viral nucleocapsid assembly,[18] and

*Correspondence to: Nick V Grishin; Email: grishin@chop.swmed.edu
Submitted: 04/01/2015; Revised: 06/23/2015; Accepted: 06/26/2015
http://dx.doi.org/10.1080/15384101.2015.1068472

VP40 is essential for virus budding and assembly.[26-28] In addition, GP, VP24, VP30, VP35 and VP40 interact with multiple host proteins to complete the viral life cycle and to suppress the host immune response.

Three-dimensional (3D) structures are available for a number of *Ebolavirus* proteins. Interpreting available experimental data and sequence variation among *Ebolavirus* species in the context of the 3D structures not only allows researchers to understand detailed mechanisms for cell entry, virus assembly and immune suppression, but also provides promising leads for structure-based drug design. In the current study, we predict the 3D structure and functional sites for *Ebolavirus* protein domains that are not yet characterized. In addition, we compare sequences of *Ebolavirus* proteins' interacting partners from RESTV-resistant primates with those from RESTV-susceptible monkeys. Elevated sequence divergence for GP and VP35's interaction partners suggests that these 2 viral proteins may be responsible for host specificity in RESTV. Finally, we compare the protein sequences from different *Ebolavirus* species to detect positions that are conserved among human pathogenic species but different in non-pathogenic RESTV (RESTV-specific mutations). Mapping of these RESTV-specific mutations and known functional sites to the 3D structures reveals clusters of RESTV-specific mutations on the surfaces of GP, VP35 and VP24. These clusters do not overlap with the known functional sites and may suggest novel interaction sites with host proteins.

Materials and Methods

Sequence analysis of *Ebolavirus* proteins

The protein sequences of *ZEBOV* were downloaded from the UniProt database[29] and submitted to the MESSA web server[30] to predict the secondary structure,[31,32] disordered regions,[33-36] transmembrane helices,[37-41] signal peptides,[38,39,42] coiled coils[43] and detect structure templates.[44,45] The 3D structures are mostly known, except for protein L, the N-terminal zinc-finger domain of VP30 and the coiled-coil region of VP35. For proteins and domains without known structure, we considered putative structural templates detected by HHpred,[45] iTASSER[46,47] and known structures for proteins of similar function from other families of RNA virus in PDB and ECOD databases.[48] Once a candidate structural template was detected, we further validated its relationship to the *Ebolavirus* protein by similarity in function, compatibility between the predicted secondary structure[49] of the *Ebolavirus* protein and the 3D structure of the template, conservation of residues in the *Ebolavirus* protein that were aligned to the active sites of the template, and the consistency among multiple structural templates. Sequences of the structural templates and the ZEBOV protein were aligned by Promals3D[50,51] and the alignments were manually adjusted to ensure that the corresponding secondary structure elements in different templates were aligned together. Based on these alignments and knowledge about functional sites in the template structures from literature, the active sites of the uncharacterized *Ebolavirus* domains were predicted.

Identification of positions associated with human pathogenicity

We downloaded protein sequences of 124 *Ebolavirus* samples from 5 *Ebolavirus* species[4] at www.sciencemag.org/content/345/6202/1369/suppl/DC1, aligned them using MAFFT,[52] and evaluated the similarity between amino acids at a certain position using BLOSUM62 scores.[53] We considered a position in the sequence alignment to be associated with the loss of human pathogenicity if it satisfies the following 2 criteria. First, the similarity in amino acids at this position from pathogenic species is always higher than the similarity between RESTV and a pathogenic species. Second, the average similarity in amino acids at this position from 4 pathogenic species (BDBV, TAFV, SUDV and ZEBOV) is significantly (p-value < 0.05) higher than that between RESTV and pathogenic species. In order to calculate the p-value for each position, we obtained an estimate of the background distribution for the positional difference between the average sequence similarity within a group of any 4 *Ebolavirus* species (all possible combinations except the one with all 4 pathogenic species) and the average sequence similarity between a fifth species and those in the group. This distribution suggests that a difference larger than 2 is associated with p-value less than 0.05. Enrichment of these pathogenicity-associated positions in each protein was measured by a binomial test (p = total number of pathogenicity-associated positions/total length of all proteins, m = number of selected positions in this protein, N = length of this protein). These pathogenicity-associated positions and the functional sites reported in literature were further mapped to the known 3D structures of *Ebolavirus* proteins.

Results and Discussion

3D structure and functional sites prediction for *Ebolavirus* proteins

Domain diagrams of all the *Ebolavirus* proteins are shown in **Figure 1**. Variable positions among the different *Ebolavirus* species are marked as black lines above the domain diagram. The average protein sequence identity between different *Ebolavirus* species ranges from 60% to 80% (**Table S1**). *Ebolavirus* proteins contain a significant fraction (20%) of structurally disordered regions, and the fraction of variable positions in these regions is significantly higher ($p < 0.01$) than in the structurally ordered regions. The 3D structures of globular regions are mostly known (**Table S2**)[54-71] except for the N-terminal zinc-finger domain of VP30, the coiled-coil domain of VP35, and protein L. Identification and analysis of structurally characterized homologs allowed us to predict the structure of the zinc-finger domain in VP30, the overall topology of NP, and the structure and catalytic sites for the catalytic domains of protein L.

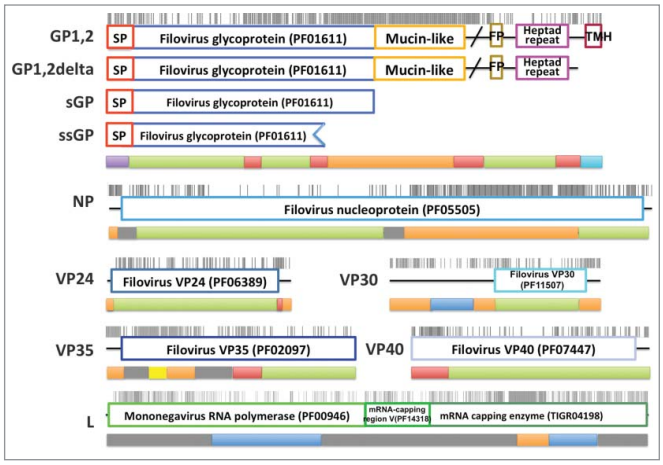

Figure 1. Domain diagrams for *Ebolavirus* proteins and coverage of the proteins by experimentally determined and predicted structures. The domains of each protein are represented by boxes on a thread and the positions that are variable among different Ebolavirus species are marked by black sticks above the domain diagrams. The band below is aligned to the domain diagram and the color of this band indicates the prediction status of the corresponding region. The color codes are: green, regions that are structurally characterized and adopt globular structure; red, regions that are experimentally determined but are intrinsically disordered; blue, regions with predicted 3D structure; yellow, coiled coil; cyan, transmembrane helix; purple, signal peptide; orange, predicted intrinsically disordered regions; gray, predicted regions that have a propensity to adopt global structure but 3D structure cannot be predicted;. Abbreviations: SP, signal peptide; FP, fusion peptide; TMH, transmembrane helix.

The zinc-finger domain of VP30

The zinc-finger domain of VP30 binds zinc[72] and contains a conserved C-x8-C-x4-C-x3-H motif. A search using the VP30 zinc finger motif (residues 70–95) as a query against the SUPERFAMILY[73] database with HHpred web server (MSA generation method: HHblits, Maximal MSA Generation iterations: 3, Score secondary structure: yes, Alignment mode: local) reveals similarity (Probability: 52.4; Identity: 35%; E-value: 2.2) to the CCCH zinc finger superfamily (seed: SCOP domain d1m9oa_). Although this is not the best hit according to HHpred probability, it has the highest coverage and is the only one (probability cutoff: 20) that contains all the zinc-binding residues. In addition, a scan of PDB sequences with the conserved pattern C-x(8)-C-x(4)-C-x(3)-H using ScanProsite[74] reveals exactly the same motif in CCCH zinc fingers (PDB id: 2d9n). All the CCCH zinc fingers belongs to one homologous group in the ECOD database,[48] and this family contains the N-terminal domain of the transcription antiterminator M2-1 from another *Mononegavirales, Pneumovirus* (4C3B[75] and 4CS7,[76] alignment shown in **Fig. S1**). In addition to their common function, the C-terminal domain of M2-1 and *Ebolavirus* VP30 share the same topology (**Fig. 2A, B**). M2-1 uses a C-x7-C-x5-C-x3-H motif to bind zinc, which is connected to an α-helix at its C-terminus. The VP30 zinc-finger domain very likely adopts a similar structure (**Fig. 2C, D**), as supported by the presence of a similar C-x8-C-x4-C-x3-H motif and a predicted α-helix following the motif.

The N-terminal domain of NP

NP has 2 structural domains that are connected by a long disordered linker of about 240 amino acids. The C-terminal domain (PDB id: 4QAZ) is shared among *Filoviridae* and is involved in protein-protein interaction.[54] The N-terminal domain is likely shared among *Mononegavirales.* Known 3D structures of NP from several virus families[77-81] in this order possess the same topology (**Fig. 3A–D**). Structures of NP from *Rhabdoviridae* and *Paramyxoviridae* families are determined in complex with ssRNA (**Fig. 3A, C**), and they both clamp around the RNA using positively charged grooves (**Fig. 3G, H**) between the 2 subdomains after a remarkable conformational change compared to the RNA-free form (**Fig. 3C, D**). The RNA-bound NPs oligomerize to form a ring (**Fig. 3I, J**), but the oligmerization interfaces vary: *Rhabdoviridae* pack the ssRNA inside the ring formed by NPs while ssRNA binds on the outside of the NP oligomer in *Paramyxoviridae*.

We predicted that the N-terminal domain of *Ebolavirus* NP adopts the same conserved topology as the other viral NPs and suggested that its structure is similar to the NP from *Nipah virus* (PDB id: 4CO6).[81] The 3D structure of this domain was released while our manuscript was under review and supported our prediction (**Fig. 3E, F**). The available 3D structures for *Ebolavirus* NP[71,82] were all determined in the absence of RNA. But its similarity to the NPs of other *Mononegavirales* and the presence of a positively charged groove between the 2 subdomains suggest a similar RNA binding mode.

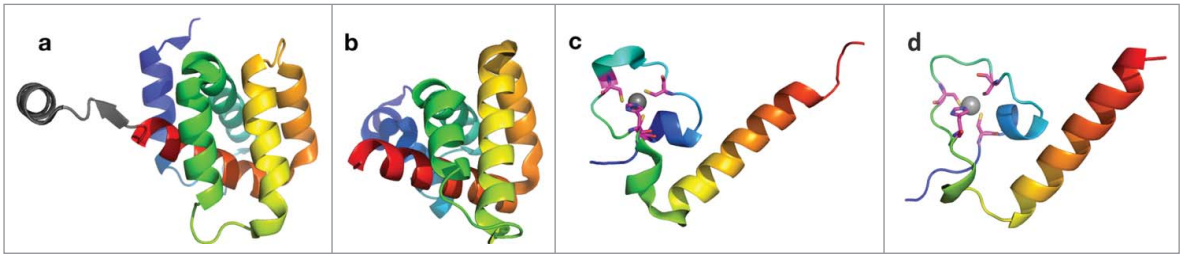

Figure 2. Structure prediction for N-terminal domain of VP30. (**A**) 3D structure (PDB id: 2I8B) for VP30 C-terminal domain; (**B**) 3D structure (PDB ID: 4C3B) for *Pneumovirus* M2-1 C-terminal domain; (**C**) 3D structure (PDB ID: 4C3B) for *Pneumovirus* M2-1 N-terminal domain, which was used as template to predict the structure for the VP30 N-terminal domain; (**D**) structure model for the *Ebolavirus* VP30 N-terminal domain.

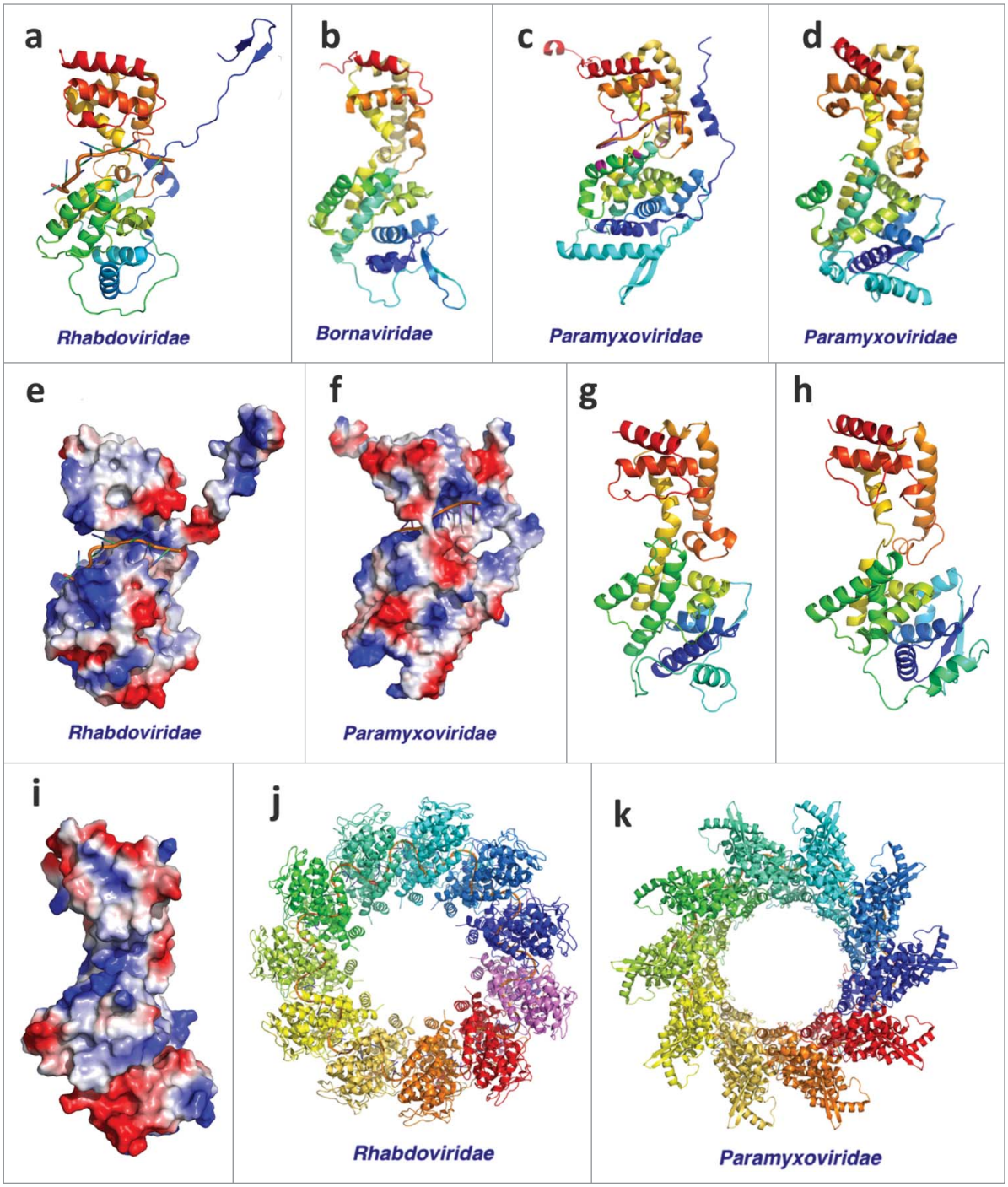

Figure 3. Structures of *Mononegavirales* Nucleoproteins. The virus family is labeled below. (**A–D**) Monomeric structures (PDB IDs: 2GIC, 1N93, 2WJ8, and 4CO6) of Nucleoproteins from *Mononegavirales*. The structures are colored in rainbow; (**E, F**) The electrostatic potential mapped onto the surface of Nucleoprotein structures (PDB ids: 2GIC and 2WJ8). Blue area corresponds to positively charged surface and the red area corresponds to negatively charged surface; (**G**) Structure model for the N-terminal domain of *Ebolavirus* NP; (**H**) Experimental structure of the N-terminal domain of *Ebolavirus* NP (PDB id: 4YPI); (**I**) The electrostatic potential mapped on to the surface of the experimental structure of the N-terminal domain of *Ebolavirus* NP; (**J, K**) Structure complex of RNA and Nucleoproteins from *Rhabdoviridae* and *Paramyxoviridae* (PDB ids: 2GIC and 2WJ8).

The RNA-dependent RNA polymerase catalytic domain of protein L

Sequence analysis suggests that the N-terminal half of protein L functions as a RNA-dependent RNA polymerase (RdRP), and is responsible for both DNA replication and transcription. HHpred[45] detects the *Bunyavirus* RdRP (PDB id: 5AMR[83]) as a structural template (Probability: 84%). The alignment between *Ebolavirus* RdRP and *Bunyavirus* RdRP

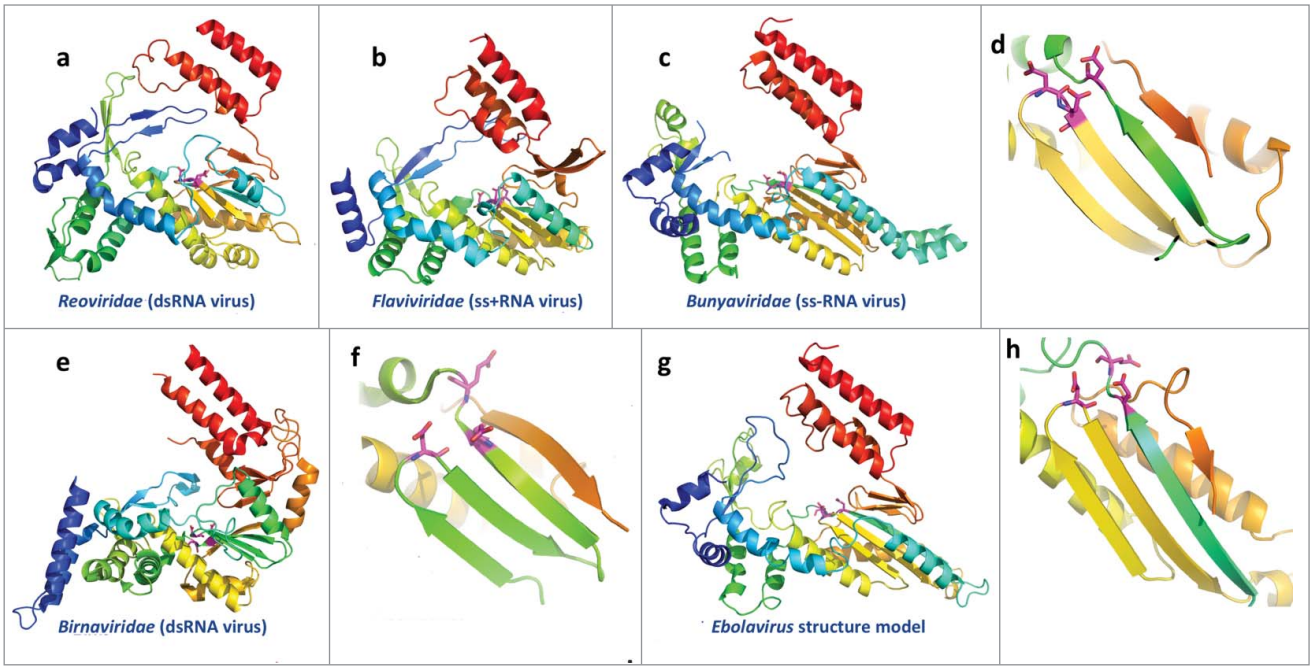

Figure 4. Structures of the catalytic domains of RNA-dependent RNA polymerases (RdRP) from RNA viruses and the structure model for *Ebolavirus* RdRP. The virus family is labeled below. The structures are colored in rainbow, with equivalent secondary structure elements from different structures colored similarly, except for the *Birnaviridae* RdRP, which has a circularly permutated topology. The functional sites used to coordinate Mg^{2+} are shown as sticks and colored in magenta. (**A–C**) Overall structure of the core domains of RdRPs from RNA viruses (PDB IDs: 2R7O, 1GX5, and 5AMR); (**D**) close up view of the classic arrangement of functional sites for the core domains of RdRPs from RNA viruses; (**E–F**) overall structure and close up view of the functional sites for the RdRP from *Birnaviridae* (dsRNA virus); PDB id: 2PGG; (**G–H**) structure model for the core domains of ZEBOV RdRP and close up view of the predicted active sites.

includes both the catalytic domain and a helical bundle connected to its C-terminus. These two domains are conserved among known structures of RdRPs from RNA viruses[84-88] (**Fig. 4A–C**). Known RdRPs from RNA viruses share the same topology except for *Birnavirus* RdRP, which has a circular permutation in the catalytic domain. This structural conservation of RdRPs across different groups of RNA virus suggests that the RdRP of *Ebolavirus* also adopts the same topology. Secondary structure prediction for the *Ebolavirus* RdRP is consistent with the topology adopted by most RNA viruses, but not with the circular permuted structure from *Birnavirus* (**Fig. 4E**).

Multiple sequence alignment and 3D structures suggest a conserved catalytic mechanism of RdRP from RNA viruses. Two conserved Asp residues that are used to coordinate Magnesium ions in the catalytic site are in the same position in the 3D structures[89] (**Fig. 4**). A sequence alignment of these RdRPs (**Fig. S2**) allows us to predict the catalytic sites for *Ebolavirus* RdRPs: D632D and D742. These two positions are conserved among close homologs of *Ebolavirus* RdRP detected by PSI-BLAST.[90] The second conserved Asp residue immediately follows a conserved Gly residue, forming a GD motif. Another Asp residue after the GD motif also participates in coordinating Mg^{2+} in most of the templates (**Fig. 4D**). However, this residue is not conserved in *Ebolavirus* and *Birnavirus* RdRPs. Alternatively, *Birnavirus*

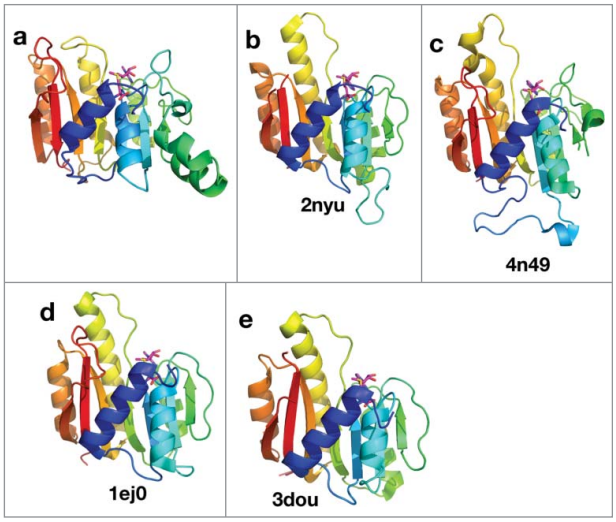

Figure 5. Structural model and templates for the mRNA capping methyltransferase domain in *Ebolavirus* protein L. The structures are colored in rainbow. Equivalent secondary structure elements from different structures are colored in the same color. The co-factor, S-adenosyl-L-methionine, is shown as sticks. (**A**) structure model for the mRNA capping methyltransferase domain of ZEBOV; (**B–E**) experimental structures of other methyltransferase domains.

Table 1. Host proteins that functionally interact with Ebolavirus proteins, and their divergence level between RESTV-susceptible and RESTV-resistant species

Name	Host protein	Functional implication	Chlorocebus vs Macaca	Homo vs Macaca
GP	NPC1[13,14]	Receptor for the virus	6 (99.5%)	28 (97.8%)
GP	TIM-1[99]		11 (96.5%)***	56 (80.2%)***
GP	CD209 [100,101]	Facilitate cell entry in specific cell types	15 (95.9%)***	31 (92.1%)***
GP	CLEC4M [100,101]		Not available in Macaca and Chlorocebus	
GP	CLEC10A[93]		5 (98.4%)	42 (86.7%)
GP	FOLR1[102]		3 (98.8%)	8 (96.9%)
GP	FURIN[7,8]	Process GP to GP1,2	1 (99.9%)	9 (98.9%)
GP	CTSB[103]	Process GP1,2 and initiate membrane fusion	2 (99.4%)	10 (97.0%)
GP	CTSL[103]		3 (99.1%)	14 (95.8%)
GP	ADAM17[9]	Process GP1,2 to GP1,2delta	1 (99.9%)	3 (99.6%)
GP	Dynamin (multiple)[104]	Activates endothelial cells, reduces their barrier function	0∼1 (99.9100%)	2∼6 (99.399.8%)
GP	ITGAV[104]		2 (99.8%)	9 (99.1%)
VP24	STAT1[61]	Inhibit JAK-STAT pathway for interferon sensing	0 (100%)	5 (99.3%)
VP24	KPNA5[56]		0 (100%)	2 (99.6%)
VP24	MAPK14 (p38)[105]	Prevent phosphorylation and inhibit interferon sensing	0 (100%)	1 (99.6%)
VP30	PPP1C[21]	Dephosphorylate VP30, control replication-transcription switch	0 (100%)	0 (100%)
VP30	PPP2C[21]		0 (100%)	0 (100%)
VP30	Dicer[106]	Antagonize RNAi machinery that could target viral RNA	5 (99.7%)	10 (99.5%)
VP30	TRBP[106]		2 (99.5%)	3 (99.2%)
VP35	Dicer[106]	Antagonize RNAi machinery that could target viral RNA	5 (99.7%)	10 (99.5%)
VP35	TRBP[106]		2 (99.5%)	3 (99.2%)
VP35	ILF3 (DRBP76)[107]	Inhibit the effect of interferon	0 (100%)	3 (99.7%)
VP35	IKBKε[108]	Block phosphorylation of IRF-3 by TBK-1 and IKBKε, inhibiting interferon production	4 (99.4%)	15 (97.9%)
VP35	TBK-1[108]		2 (99.7%)	8 (98.9%)
VP35	IRF-3[108]		2 (99.5%)	17 (96.0%)
VP35	PACT[109]	Inhibit its role as RIG-I activator	0 (100%)	0 (100%)
VP35	PKR[110]	Inhibit the effect of interferon	42 (92.4%)***	110 (80%)***
VP35	UBE2I[111]	Use SUMO E2 enzyme (UBE21) and E3 ligase (PIAS1) to modify IRF7 and inhibit its function	0 (100%)	0 (100%)
VP35	PIAS1[111]		0 (100%)	0 (100%)
VP35	IRF-7[111]		9 (98.2%)	35 (92.9%)
VP35	DLC8[112]	May regulate viral life cycle	1 (98.9%)	0 (100%)
VP40	Sec24C[113]	Virus utilize COPII vesicular transport system for life cycle	7 (99.4%)	24 (97.8%)
VP40	TSG101[28]	Virus uses multi-vesicular body biogenesis pathway for budding	0 (100%)	0 (100%)
VP40	ABL1[114]	ABL1 controls budding/release by phosphorylating VP40	5 (99.6%)	13 (98.8%)
VP40	NEDD4[115]	NEDD4 facilitates budding by adding ubiquitin to VP40	5 (99.5%)	28 (97.8%)
VP40	Tubulin (multiple)[116]	Virus utilize host cytoskeleton in its life cycle	0 (100%)	0 (100%)
VP40	Actin (1 and 2)[117]		0 (100%)	0 (100%)
VP40	IQGAP1[118]		2 (99.9%)	9 (99.4%)

***significantly ($p<0.05$) elevated divergence level.

RdRP has a Glu residue after the first conserved Asp (**Fig. 4F**), which is in the correct position to bind Mg^{2+}. Similarly, a conserved Glu residue (634E) in the same position in the *Ebolavirus* RdRP may participate in Mg^{2+} binding, and the arrangement of these active site residues likely resembles that in *Birnavirus* RdRP.

The methyltransferase domain of protein L for mRNA capping

Addition of a 7-methylguanosine cap to the 5′ end of mRNA is essential for its subsequent translation and stability in eukaryotic cells.[91] The C-terminal half of protein L is responsible for mRNA capping, and it contains an S-adenosyl-L-methionine-dependent methyltransferase domain that likely works in this process. HHpred detects several structural templates (**Fig. 5**) for this domain with probabilities above 95%. A sequence alignment between the *Ebolavirus* methyltransferase domain and the detected templates (**Fig. S3**) reveals that 3 residues, K1816, D1927, and K1962, are aligned to the conserved catalytic residues in the templates.[92] In addition, the "GEGAGA" motif at positions 1836–1841 of *Ebolavirus* protein L is aligned to the conserved S-adenosyl-L-methionine-binding motif in the templates. This motif is also conserved in sequences from *Filoviridae*, suggesting a similar function in co-factor binding.

Interaction between *Ebolavirus* proteins and host proteins

RESTV causes EHF symptoms to Asian cynomolgus monkeys (*Macaca fascicularis*), but not human and African green monkeys (*Chlorocebus aethiops*).[5] This difference in susceptibility between closely related hosts is likely due to the sequence divergence in the host proteins that interact with virus proteins. Therefore, comparing the interacting partners of virus proteins from different hosts may provide insight into how host specificity is determined and further suggest the mechanism for RESTV's loss of human pathogenicity. The known interacting partners in the host for each *Ebolavirus* protein are summarized in **Table 1**.

The known host proteins that interact with VP24, VP30, and VP40 are highly similar between the RESTV-resistant (*Chlorocebus* and human) and RESTV-susceptible species (*Macaca*), suggesting that they may not be responsible for RESTV's loss of human pathogenicity. In contrast, 7 most divergent host partners interact either with GP or VP35. Three of them (marked in **Table 1**) show significantly ($P < 0.05$) elevated divergence between the susceptible and resistant species, including Hepatitis A virus cellular receptor 1 (TIM-1) and pathogen-recognition receptor CD209 that interact with GP and facilitates cell entry, as well as the interferon-induced, dsRNA-activated kinase PKR that is inhibited by VP35.

Table 2. Positions in ZEBOV that are likely associated with the loss of human pathogenicity by RESTV

Name	UniProt ID	Length	P-value	Mutations associated with the loss of human pathogenicity
GP	Q05320	676	0.457	F31I, Q44K, V45A, E156N, S196A, L199A, S210T, Y261R, T269S, T283P, S307H, T335P, E337T, H339N, E345T, H354L, E359T, A361E, A427M, G488K, R498K, R500K, N514D, D607S, K622E, I627K, Q638H, D642L, W644L, T659I
L	Q05318	2212	0.690	V66T, E93T, Q109H, N120A, V128T, E130I, F132T, L146V, L179F, N201T, T202I, A221S, Q223L, H227Q, V229L, P262V, V263D, S274L, L283V, Y312F, A326S, T330D, S343Y, E350D, T361S, L365F, I402N, Q447H, P450S, D465N, R654H, E689S, S847A, S868A, F896Y, L925F, A954S, S995T, T1024N, R1073K, A1119S, Q1149P, S1154L, P1163A, K1171D, D1189S, A1214S, R1217K, D1237E, Q1253N, Y1322L, R1354K, T1366A, I1408M, S1436N, K1461Q, S1473C, L1488Y, S1506A, A1538S, V1562L, E1564S, T1571K, Q1608I, H1619L, L1624Y, C1628S, D1744G, E1752P, S1769G, Q1782L, R1792H, W1822L, V1850T, R1916N, K1938Q, E1941R, V1955Y, Q2024G, P2038V, S2077T, K2078G, R2079L, E2098D, Q2105L, Q2108E, Y2131F, L2157V, R2168H, R2175K, L2177F, M2186L, L2203F
NP	P18272	739	0.587	R4G, T15G, S30T, R39K, I52M, R105K, M137L, F212Y, K274R, S279A, K373R, K374R, A411L, K416N, Y421Q, D426E, D435N, Q442L, D443E, T453I, V458A, D492E, Q507S, S511I, N551R, T563S, E633L, S647K, A705R, T714Y, D716N
VP24	Q05322	251	0.932	T131S, N132T, M136L, Q139R, T226A, S248L
VP30	Q05323	288	0.010	G20P, V25S, Y39R, T52N, V53L, T63I, E93D, T96N, R98H, K107R, S111I, L116S, N117Q, A120S, Q135S, T150I, Q157R, R196H, E205D, R262A, S268Q
VP35	Q05127	340	0.019	T5L, L25T, S26T, E48D, D76E, C79Y, N80V, E85K, S92M, V97T, Q98S, S106A, A154S, T159V, E160D, G167K, S174A, I258T, E269D, A290V, A291P, V314A, Q329K
VP40	Q05128	326	0.786	M14N, T46V, P85T, A128I, G201N, F209L, Q245P, H269Q, T277Q, V323H, E325D

P-value: binomial test for enrichment of residues that may be associated with RESTV's loss of human pathogenicity in each protein.

The elevated divergence level for interacting partners of GP and VP35 in the host suggests that VP35 and GP may play important roles in determining host specificity. This is consistent with some indirect experimental data. RESTV GP pseudotyped viruses show significantly lower ability to infect human cells and to damage human endothelial cells than that of ZEBOV GP pseudotyped viruses.[93] In addition, RESTV GP shows lower ability to deplete T cells and to down-regulate interferon-stimulated gene expression compared to ZEBOV GP.[94,95] Meanwhile, ZEBOV VP35 shows stronger Interferon inhibition than RESTV VP35 in human cells.[68] However, direct studies of all RESTV proteins' effect in cells of both RESTV-susceptible and RESTV-resistant species are needed to prove our hypothesis.

Interpreting residues associated with RESTV's loss of human pathogenicity in the context of 3D structure and known functional sites

We consider positions that are associated with the loss of pathogenicity in RESTV as those that are always and significantly more similar among pathogenic species (BDBV, TAFV, SUDV and ZEBOV) than between RESTV and the pathogenic species. We referred to them as "RESTV-specific mutations." We

Table 3. Experimentally characterized functional sites in *Ebolavirus* proteins

Name	Residues	Function	Experimental evidence
GP	40	Glycosylated by host	N40D loss ability to infect[119]
GP	41–43, 503–511, 513, 514	Interact with antibody	On the interacting surface with neutralizing antibody [55]
GP	51, 68, 86, 99, 109,111, 113, 122, 139, 154, 159, 161, 162, 171, 176, 183–185	Maintain the hydrophobic core structure	W86A, Y99A, Y109A, H139A, H154A, F159A, L161A, Y162A, Y171A, F176A, F183A reduce expression, reduce viral incorporation and abolish infectivity; L111A, I113A, L122A reduce viral incorporation and abolish infectivity; L51A, L68A, L184A, I185A abolish infectivity[120]
GP	53, 108, 121, 135, 147, 511, 556, 601, 608, 609	Disulfide bond	C53G, C108A, C121G, C135S, C147S, C511G, C556S, C601S, C608G, C609G reduce expression and abolish infectivity[119]
GP	55, 85, 103, 117, 178	Hydrophilic to maintain the structure	E85A, E103A, E178A reduce expression; E85A, E103A, D117A, E178A reduce viral incorporation; D55A, E103A, D117A, E178A loss ability to infect[120]
GP	529, 531–533, 535–537	Fusion peptide	I529A, W531R, W531A, I532R, P533R, F535R, G536R, G536A, P537R loss ability to infect[15]
GP	57, 63, 64, 88, 95, 170	Cell entry	L63K, L63A reduce expression; L57A, L57F, L57I, L57K, L63K, L63A, L63F, R64E, R64A, F88E, F88A, K95E, K95A, I170A, I170E loss ability to infect[120]
VP24	96–98, 106–121	Interact with STAT1	Show reduced hydrogen exchange rate upon binding[61]
VP24	113, 115, 117, 121, 124, 125, 128–131, 134–141, 184–186, 201–205, 218	Interact with KPNA5	On the interacting surface in crystal structure with KPNA5 (PDB id: 4U2X)[56]
VP24	50, 71, 147, 187	Adapt to new host	T50I mouse adaptation[98]; M71I, L147P, and T187I guinea pig adaptation[97]
VP30	179, 180, 183, 197	Activate transcription	Mutation to Ala reduces interaction with nucleocapsid; K180A, K183A, E197A block transcription activation[59]
VP30	143, 146	Phosphorylation	T143A, T143D, T146A, T146D inhibit transcription[21]
VP35	239, 240, 309, 312, 319, 322, 339	Bind dsRNA	K309A, K319A reduce dsRNA binding; F239A, H240A, R312A, R322A, K339A abolishes dsRNA binding[70]
VP35	239, 240, 309, 312, 319, 322, 339	IRF-3 inhibition	K309A, K319A reduce IRF-3 inhibition; F239A, H240A, R312A, R322A, K339A greatly reduce IRF-3 inhibition[70]
VP35	235, 240	Polymerase cofactor	F235A, H240A impair replication of mini-genome[24]
VP35	312, 322, 339	Bind DRPB76	Mutation to alanine reduce ability to bind DRPB76[107]
VP35	309, 312	Inhibit RNAi	K309A and R312A lost the inhibition effect[121]
VP35	305, 309, 312	Inhibit PKR	Mutant any 2 to alanine abolish the inhibition[122]
VP40	303–308	Interact with Sec24C	303–306A and 305–308A cannot interact with Sec24C, and reduce virus-like particles[113]
VP40	51–54, 96–101, 212–214, 286–291, 303–308, 314–316	Release of virus-like particles	51–52A, 53–54A, deletion of 96–101, K212A, L213A, R214A, 286–288A, 289–291A, 303–306A, 305–308A reduce the release of virus-like particles[113,123,124]
VP40	127, 129, 130, 283, 286, 293, 295, 298, 309–317	Membrane localization	K127A, T129A, N130A, P283L, P286L, I293A, L295A, V298A and deletion of 309–317 reduce membrane localization[27, 125]
VP40	226–255	Interaction with microtubules	Deletion of 226–240 or 241–255 abolish ability to protect microtubules from depolymerization[116]
VP40	213, 293, 295, 298	Penetrate membrane	Mutation to alanine reduces membrane localization[126]

identified 215 such positions (**Table 2**), and VP30 and VP35 are significantly enriched in such mutations.

43 of the RESTV-specific mutations can be mapped to known 3D structures of *Ebolavirus* proteins. None of them overlap with functional sites that are proved to be crucial by mutagenesis and 6 of them overlap with interaction surfaces (summarized in **Table 3**) on these structures. They may affect the binding affinities but would not likely abolish the interactions. One loop (129–141) of VP24 at the boundary of the interacting surface between VP24 and KPNA5[50] contains 4 RESTV-specific mutations (T131S, N132T, M136L, Q139R, within the red circle in **Fig. 6C**). These mutations may affect the binding affinity between RESTV and KPNA5 in RESTV, weakening the immune suppression by RESTV. One mutation to GP (N514D) is at the boundary of its interacting surface with neutralizing antibodies from a human survivor[55] and this mutation may affect the efficiency of the ZEBOV antibodies to antagonize RESTV.

Mapping of the RESTV-specific mutations to the 3D structures revealed a couple of mutation clusters in GP and VP35, which may be related to RESTV's difference in pathogenicity (**Fig. 6**). A first cluster is in the C-terminal subdomain of GP. The cluster consists of 3 mutations on the surface: Y261R, T269S, and S307H (inside the blue circle in **Fig. 6A**). The functional role of this subdomain is not clear, and the cell entry of ZEBOV is mostly mediated by the interaction between N-terminal 150 residues of GP and cell receptors like NPC1 and TIM-1.

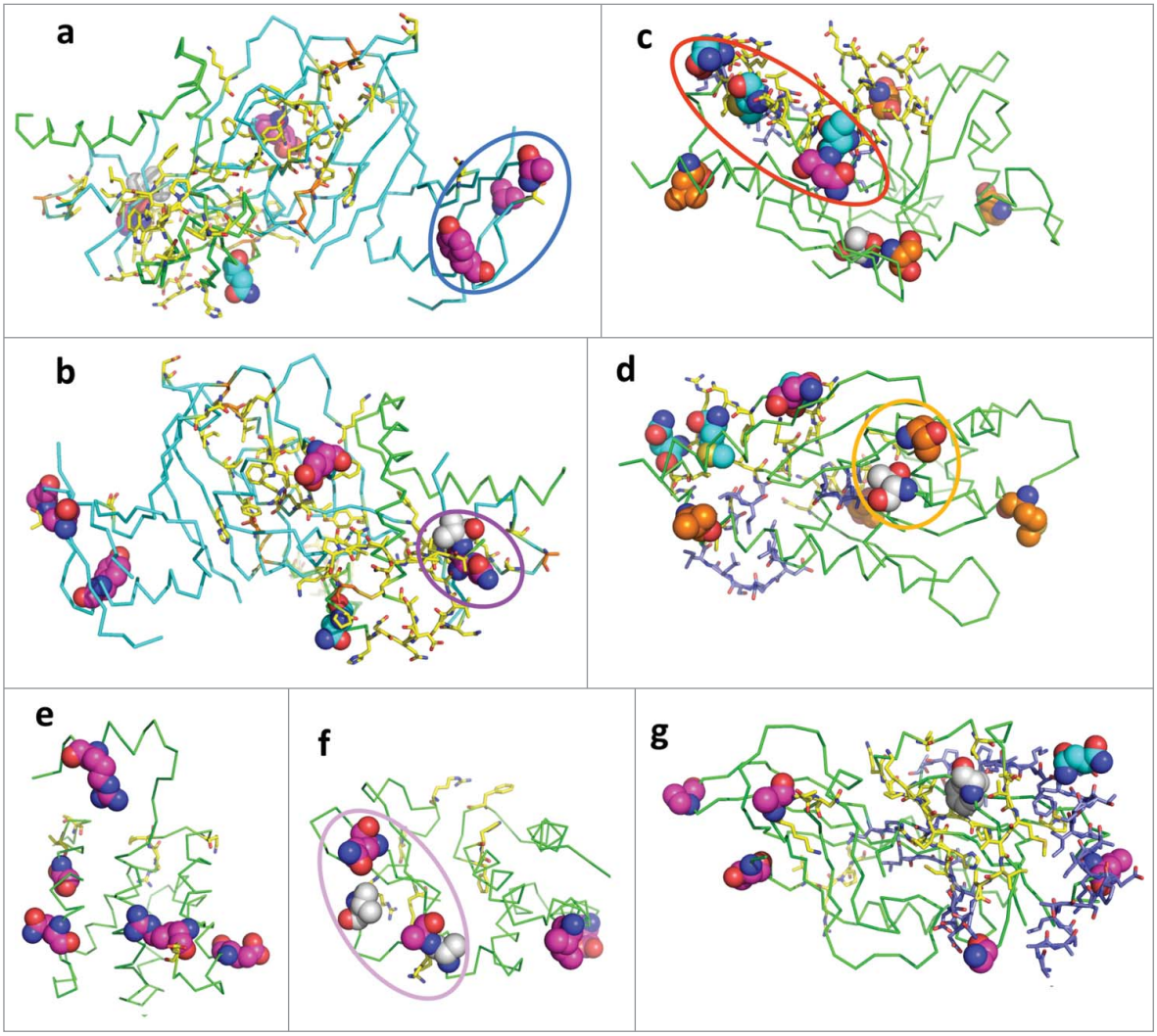

Figure 6. Mapping of RESTV-specific residues, functional sites and interaction surfaces to known 3D structures of *Ebolavirus* proteins. The structure is shown in ribbon; the functional sites are shown as sticks; and positions with RESTV-specific mutations and alternate host (rodent) adaptation residues are shown as spheres. Carbon atoms of the functional sites and sites with RESTV-specific mutations are colored to show the property of that residue: RESTV-specific surface residues are in magenta; RESTV-specific buried residues are in white; RESTV-specific residues that belong to interaction surfaces are in cyan; known functional sites are in yellow; disulfide bonded and alternate host (rodent) adaptation residues are in orange; predicted functional residues are in blue. Other atoms are colored as follows: oxygen (red); nitrogen (blue) and sulfur (orange). Circles highlight clusters of RESTV-specific residues that are discussed in the text. (**A, B**) GP (PDB id: 3CSY); (**C, D**) VP24 (PDB id: 4U2X); (**E**) VP30 (PDB id: 2I8B); (**F**) VP35 (PDB id: 3L26); (**G**) VP40 (PDB id: 1ES6).

One possibility is that it may interact with other host proteins, such as lectins that facilitate the infection of Ebolavirus. In contrast, another cluster of mutations (Q44K, and V45A, inside the magenta circle in **Fig. 6B**) may affect the interaction between GP and the cell receptors. Even more, the mutation E156N is close to functional sites that are shown by mutagenesis to be important for maintaining the infectivity of ZEBOV. Therefore, these RESTV-specific mutations of GP may cause a significantly lower infectivity in RESTV and contribute to the loss of human pathogenicity.

RESTV-specific mutations (A290V, A291P, V314A, and Q329K) in VP35 form a cluster (inside the pink circle in **Fig. 6F**) on the opposite side of the dsRNA-binding surface of VP35. Host immune suppression by VP35 is mainly related to its interaction with dsRNA, but the loss of dsRNA-binding ability does not completely abolish VP35-mediated immune suppression.[96] This observation indicates the existence of other mechanisms for immune suppression by VP35, where the surface enriched in RESTV-specific mutations may play a role. One RESTV-specific mutation (T226A) is adjacent to the position in VP24 that is mutated (T50I) during adaptation to mice[97,98] (orange circles in **Fig. 6D**). This adaptation site is not close to any known functional sites, but the clustering of the adaptation site and RESTV-specific mutation suggests the possibility that they are at the interface of some uncharacterized interaction with other host proteins.

Disclosure of Potential Conflicts of Interest

No potential conflicts of interest were disclosed.

Acknowledgments

We thank Drs. R. Dustin Schaeffer and Lisa N. Kinch for critical reading of the manuscript. Qian Cong is a Howard Hughes Medical Institute International Student Research fellow.

Funding

This work was supported in part by the National Institutes of Health (GM094575 to NVG) and the Welch Foundation (I-1505 to NVG).

Supplemental Material

Supplemental data for this article can be accessed on the publisher's website.

References

1. Organization WH. 2014. Ebola virus disease Fact Sheets: http://www.who.int/mediacentre/factsheets/fs103/en/
2. Organization WH. 2015. Ebola data and statistics (published on 18 February 2015): http://apps.who.int/gho/data/view.ebola-sitrep.ebola-summary-20150218?lang=en
3. Kuhn JH, Becker S, Ebihara H, Geisbert TW, Johnson KM, Kawaoka Y, Lipkin WI, Negredo AI, Netesov SV, Nichol ST, Palacios G, et al. Proposal for a revised taxonomy of the family Filoviridae: classification, names of taxa and viruses, and virus abbreviations. Arch Virol 2010; 155:2083-103; PMID:21046175; http://dx.doi.org/10.1007/s00705-010-0814-x
4. Gire SK, Goba A, Andersen KG, Sealfon RS, Park DJ, Kanneh L, Jalloh S, Momoh M, Fullah M, Dudas G, et al. Genomic surveillance elucidates Ebola virus origin and transmission during the 2014 outbreak. Science 2014; 345:1369-72; PMID:25214632; http://dx.doi.org/10.1126/science.1259657
5. Morikawa S, Saijo M, Kurane I. Current knowledge on lower virulence of Reston Ebola virus (in French: Connaissances actuelles sur la moindre virulence du virus Ebola Reston). Compar Immunol Microbiol Infect Dis 2007; 30:391-8; PMID:17610952; http://dx.doi.org/10.1016/j.cimid.2007.05.005
6. Sanchez A, Trappier SG, Mahy BW, Peters CJ, Nichol ST. The virion glycoproteins of Ebola viruses are encoded in two reading frames and are expressed through transcriptional editing. Proc Natl Acad Sci U S A 1996 93:3602-7; PMID:8622982; http://dx.doi.org/10.1073/pnas.93.8.3602
7. Volchkov VE, Feldmann H, Volchkova VA, Klenk HD. Processing of the Ebola virus glycoprotein by the proprotein convertase furin. Proc Natl Acad Sci U S A 1998; 95:5762-7; PMID:9576958; http://dx.doi.org/10.1073/pnas.95.10.5762
8. Wool-Lewis RJ, Bates P. Endoproteolytic processing of the ebola virus envelope glycoprotein: cleavage is not required for function. J Virol 1999 73:1419-26; PMID:9882347
9. Dolnik O, Volchkova V, Garten W, Carbonnelle C, Becker S, Kahnt J, Stroher U, Klenk HD, Volchkov V. Ectodomain shedding of the glycoprotein GP of Ebola virus. EMBO J 2004; 23:2175-84; PMID:15103332; http://dx.doi.org/10.1038/sj.emboj.7600219
10. Mehedi M, Falzarano D, Seebach J, Hu X, Carpenter MS, Schnittler HJ, Feldmann H. A new Ebola virus nonstructural glycoprotein expressed through RNA editing. J Virol 2011; 85:5406-14; PMID:21411529; http://dx.doi.org/10.1128/JVI.02190-10
11. Volchkova VA, Feldmann H, Klenk HD, Volchkov VE. The nonstructural small glycoprotein sGP of Ebola virus is secreted as an antiparallel-orientated homodimer. Virology 1998; 250:408-14; PMID:9792851; http://dx.doi.org/10.1006/viro.1998.9389
12. Mohamadzadeh M, Chen L, Schmaljohn AL. How Ebola and Marburg viruses battle the immune system. Nat Rev Immunol 2007; 7:556-67; PMID:17589545
13. Carette JE, Raaben M, Wong AC, Herbert AS, Obernosterer G, Mulherkar N, Kuehne AI, Kranzusch PJ, Griffin AM, Ruthel G, et al. Ebola virus entry requires the cholesterol transporter Niemann-Pick C1. Nature 2011; 477:340-3; PMID:21866103; http://dx.doi.org/10.1038/nature10348
14. Miller EH, Obernosterer G, Raaben M, Herbert AS, Deffieu MS, Krishnan A, Ndungo E, Sandesara RG, Carette JE, Kuehne AI, et al. Ebola virus entry requires the host-programmed recognition of an intracellular receptor. EMBO J 2012; 31:1947-60; PMID:22395071; http://dx.doi.org/10.1038/emboj.2012.53
15. Ito H, Watanabe S, Sanchez A, Whitt MA, Kawaoka Y. Mutational analysis of the putative fusion domain of Ebola virus glycoprotein. J Virol 1999; 73:8907-12; PMID:10482652
16. Gomara MJ, Mora P, Mingarro I, Nieva JL. Roles of a conserved proline in the internal fusion peptide of Ebola glycoprotein. FEBS Lett 2004; 569:261-6; PMID:15225645; http://dx.doi.org/10.1016/j.febslet.2004.06.006
17. Watanabe S, Noda T, Kawaoka Y. Functional mapping of the nucleoprotein of Ebola virus. J Virol 2006; 80:3743-51; PMID:16571791; http://dx.doi.org/10.1128/JVI.80.8.3743-3751.2006
18. Huang Y, Xu L, Sun Y, Nabel GJ. The assembly of Ebola virus nucleocapsid requires virion-associated proteins 35 and 24 and posttranslational modification of nucleoprotein. Mol Cell 2002; 10:307-16; PMID:12191476; http://dx.doi.org/10.1016/S1097-2765(02)00588-9
19. Weik M, Modrof J, Klenk HD, Becker S, Muhlberger E. Ebola virus VP30-mediated transcription is regulated by RNA secondary structure formation. J Virol 2002; 76:8532-9; PMID:12163572; http://dx.doi.org/10.1128/JVI.76.17.8532-8539.2002
20. Martinez MJ, Biedenkopf N, Volchkova V, Hartlieb B, Alazard-Dany N, Reynard O, Becker S, Volchkov V. Role of Ebola virus VP30 in transcription reinitiation. J Virol 2008; 82:12569-73; PMID:18829754; http://dx.doi.org/10.1128/JVI.01395-08
21. Ilinykh PA, Tigabu B, Ivanov A, Ammosova T, Obukhov Y, Garron T, Kumari N, Kovalskyy D, Platonov MO, Naumchik VS, et al. Role of protein phosphatase 1 in dephosphorylation of Ebola virus VP30 protein and its targeting for the inhibition of viral transcription. J Biol Chem 2014; 289:22723-38; PMID:24936058; http://dx.doi.org/10.1074/jbc.M114.575050
22. Biedenkopf N, Hartlieb B, Hoenen T, Becker S. Phosphorylation of Ebola virus VP30 influences the composition of the viral nucleocapsid complex: impact on viral transcription and replication. J Biol Chem 2013; 288:11165-74; PMID:23493393; http://dx.doi.org/10.1074/jbc.M113.461285
23. Muhlberger E, Weik M, Volchkov VE, Klenk HD, Becker S. Comparison of the transcription and replication strategies of marburg virus and Ebola virus by using artificial replication systems. J Virol 1999; 73:2333-42; PMID:9971816
24. Prins KC, Binning JM, Shabman RS, Leung DW, Amarasinghe GK, Basler CF. Basic residues within the ebolavirus VP35 protein are required for its viral polymerase cofactor function. J Virol 2010;

84:10581-91; PMID:20686031; http://dx.doi.org/10.1128/JVI.00925-10
25. Hoenen T, Jung S, Herwig A, Groseth A, Becker S. Both matrix proteins of Ebola virus contribute to the regulation of viral genome replication and transcription. Virology 2010; 403:56-66; PMID:20444481; http://dx.doi.org/10.1016/j.virol.2010.04.002
26. Han Z, Boshra H, Sunyer JO, Zwiers SH, Paragas J, Harty RN. Biochemical and functional characterization of the Ebola virus VP24 protein: implications for a role in virus assembly and budding. J Virol 2003; 77:1793-800; PMID:12525613; http://dx.doi.org/10.1128/JVI.77.3.1793-1800.2003
27. Panchal RG, Ruthel G, Kenny TA, Kallstrom GH, Lane D, Badie SS, Li L, Bavari S, Aman MJ. In vivo oligomerization and raft localization of Ebola virus protein VP40 during vesicular budding. Proc Natl Acad Sci U S A 2003; 100:15936-41; PMID:14673115; http://dx.doi.org/10.1073/pnas.2533915100
28. Martin-Serrano J, Zang T, Bieniasz PD. HIV-1 and Ebola virus encode small peptide motifs that recruit Tsg101 to sites of particle assembly to facilitate egress. Nat Med 2001; 7:1313-9; PMID:11726971; http://dx.doi.org/10.1038/nm1201-1313
29. UniProt C. UniProt: a hub for protein information. Nucleic Acids Res 2015; 43:D204-212; PMID:25348405; http://dx.doi.org/10.1093/nar/gku989
30. Cong Q, Grishin NV. MESSA: MEta-Server for protein Sequence Analysis. BMC Biol 2012; 10:82; PMID:23031578; http://dx.doi.org/10.1186/1741-7007-10-82
31. Pollastri G, Przybylski D, Rost B, Baldi P. Improving the prediction of protein secondary structure in three and eight classes using recurrent neural networks and profiles. Proteins 2002; 47:228-35; PMID:11933069; http://dx.doi.org/10.1002/prot.10082
32. Jones DT. Protein secondary structure prediction based on position-specific scoring matrices. J Mol Biol 1999; 292:195-202; PMID:10493868; http://dx.doi.org/10.1006/jmbi.1999.3091
33. Cheng J, Sweredoski M, Baldi P. Accurate prediction of protein disordered regions by mining protein structure data. Data Mining Knowl Discov 2005; 11:213-22; http://dx.doi.org/10.1007/s10618-005-0001-y
34. Linding R, Jensen LJ, Diella F, Bork P, Gibson TJ, Russell RB. Protein disorder prediction: implications for structural proteomics. Structure 2003; 11:1453-9; PMID:14604535; http://dx.doi.org/10.1016/j.str.2003.10.002
35. Ward JJ, Sodhi JS, McGuffin LJ, Buxton BF, Jones DT. Prediction and functional analysis of native disorder in proteins from the three kingdoms of life. J Mol Biol 2004; 337:635-45; PMID:15019783; http://dx.doi.org/10.1016/j.jmb.2004.02.002
36. Lobanov MY, Galzitskaya OV. 2011. The Ising model for prediction of disordered residues from protein sequence alone. Phys Biol 8:035004; PMID:21572175; http://dx.doi.org/10.1088/1478-3975/8/3/035004
37. Tusnady GE, Simon I. Principles governing amino acid composition of integral membrane proteins: application to topology prediction. J Mol Biol 1998; 283:489-506; PMID:9769220; http://dx.doi.org/10.1006/jmbi.1998.2107
38. Jones DT. Improving the accuracy of transmembrane protein topology prediction using evolutionary information. Bioinformatics 2007; 23:538-44; PMID:17237066; http://dx.doi.org/10.1093/bioinformatics/btl677
39. Kall L, Krogh A, Sonnhammer EL. A combined transmembrane topol signal peptide prediction method. J Mol Biol 2004; 338:1027-36; PMID:15111065; http://dx.doi.org/10.1016/j.jmb.2004.03.016
40. Krogh A, Larsson B, von Heijne G, Sonnhammer EL. Predicting transmembrane protein topology with a hidden Markov model: application to complete genomes. J Mol Biol 2001; 305:567-80; PMID:11152613; http://dx.doi.org/10.1006/jmbi.2000.4315
41. von Heijne G. Membrane protein structure prediction. Hydrophobicity analysis and the positive-inside rule. J Mol Biol 1992; 225:487-94; PMID:1593632; http://dx.doi.org/10.1016/0022-2836(92)90934-C
42. Bendtsen JD, Nielsen H, von Heijne G, Brunak S. Improved prediction of signal peptides: SignalP 3.0. J Mol Biol 2004; 340:783-95; PMID:15223320; http://dx.doi.org/10.1016/j.jmb.2004.05.028
43. Lupas A, Van Dyke M, Stock J. Predicting coiled coils from protein sequences. Science 1991; 252:1162-4; PMID:2031185; http://dx.doi.org/10.1126/science.252.5009.1162
44. Altschul SF, Gish W, Miller W, Myers EW, Lipman DJ. Basic local alignment search tool. J Mol Biol 1990; 215:403-10; PMID:2231712; http://dx.doi.org/10.1016/S0022-2836(05)80360-2
45. Remmert M, Biegert A, Hauser A, Soding J. HHblits: lightning-fast iterative protein sequence searching by HMM-HMM alignment. Nat Methods 2012; 9:173-5; http://dx.doi.org/10.1038/nmeth.1818
46. Zhang Y. I-TASSER server for protein 3D structure prediction. BMC Bioinfor 2008; 9:40; PMID:18215316; http://dx.doi.org/10.1186/1471-2105-9-40
47. Roy A, Kucukural A, Zhang Y. I-TASSER: a unified platform for automated protein structure and function prediction. Nat Protocols 2010; 5:725-38; PMID:20360767; http://dx.doi.org/10.1038/nprot.2010.5
48. Cheng H, Schaeffer RD, Liao Y, Kinch LN, Pei J, Shi S, Kim BH, Grishin NV. ECOD: an evolutionary classification of protein domains. PLoS Comput Biol 2014; 10:e1003926; PMID:25474468; http://dx.doi.org/10.1371/journal.pcbi.1003926
49. Cole C, Barber JD, Barton GJ. Jpred 3 secondary structure prediction server. Nucleic Acids Res 2008; 36:W197-201; PMID:18463136; http://dx.doi.org/10.1093/nar/gkn238
50. Pei J, Kim BH, Grishin NV. PROMALS3D: a tool for multiple protein sequence and structure alignments. Nucleic Acids Res 2008; 36:2295-300; PMID:18287115; http://dx.doi.org/10.1093/nar/gkn072
51. Pei J, Grishin NV. PROMALS3D: multiple protein sequence alignment enhanced with evolutionary and three-dimensional structural information. Methods Mol Biol 2014; 1079:263-71; PMID:24170408; http://dx.doi.org/10.1007/978-1-62703-646-7_17
52. Katoh K, Standley DM. MAFFT multiple sequence alignment software version 7: improvements in performance and usability. Mol biol Evolut 2013; 30:772-80; PMID:23329690; http://dx.doi.org/10.1093/molbev/mst010
53. Henikoff S, Henikoff JG. Amino acid substitution matrices from protein blocks. Proc Natl Acad Sci U S A 1992; 89:10915-9; PMID:1438297; http://dx.doi.org/10.1073/pnas.89.22.10915
54. Dziubanska PJ, Derewenda U, Ellena JF, Engel DA, Derewenda ZS. The structure of the C-terminal domain of the Zaire ebolavirus nucleoprotein. Acta crystallographica. Sec D Biol Bryst 2014; 70:2420-9; http://dx.doi.org/10.1107/S1399004714014710
55. Lee JE, Fusco ML, Hessell AJ, Oswald WB, Burton DR, Saphire EO. Structure of the Ebola virus glycoprotein bound to an antibody from a human survivor. Nature 2008; 454:177-82; PMID:18615077; http://dx.doi.org/10.1038/nature07082
56. Xu W, Edwards MR, Borek DM, Feagins AR, Mittal A, Alinger JB, Berry KN, Yen B, Hamilton J, Brett TJ, et al. Ebola virus VP24 targets a unique NLS binding site on karyopherin α 5 to selectively compete with nuclear import of phosphorylated STAT1. Cell Host Microb 2014; 16:187-200; PMID:25121748; http://dx.doi.org/10.1016/j.chom.2014.07.008
57. Edwards MR, Johnson B, Mire CE, Xu W, Shabman RS, Speller LN, Leung DW, Geisbert TW, Amarasinghe GK, Basler CF. The Marburg virus VP24 protein interacts with Keap1 to activate the cytoprotective antioxidant response pathway. Cell Rep 2014; 6:1017-25; PMID:24630991; http://dx.doi.org/10.1016/j.celrep.2014.01.043
58. Kimberlin CR, Bornholdt ZA, Li S, Woods VL, Jr., MacRae IJ, Saphire EO. Ebolavirus VP35 uses a bimodal strategy to bind dsRNA for innate immune suppression. Proc Natl Acad Sci U S A 2010; 107:314-9; PMID:20018665; http://dx.doi.org/10.1073/pnas.0910547107
59. Hartlieb B, Muziol T, Weissenhorn W, Becker S. Crystal structure of the C-terminal domain of Ebola virus VP30 reveals a role in transcription and nucleocapsid association. Proc Natl Acad Sci U S A 2007; 104:624-9; PMID:17202263; http://dx.doi.org/10.1073/pnas.0606730104
60. Bale S, Julien JP, Bornholdt ZA, Krois AS, Wilson IA, Saphire EO. Ebolavirus VP35 coats the backbone of double-stranded RNA for interferon antagonism. J Virol 2013; 87:10385-8; PMID:23824825; http://dx.doi.org/10.1128/JVI.01452-13
61. Zhang AP, Bornholdt ZA, Liu T, Abelson DM, Lee DE, Li S, Woods VL, Jr., Saphire EO. The ebola virus interferon antagonist VP24 directly binds STAT1 and has a novel, pyramidal fold. PLoS Pathog 2012; 8:e1002550; PMID:22383882; http://dx.doi.org/10.1371/journal.ppat.1002550
62. Bale S, Dias JM, Fusco ML, Hashiguchi T, Wong AC, Liu T, Keuhne AI, Li S, Woods VL Jr., Chandran K, et al. Structural basis for differential neutralization of ebolaviruses. Viruses 2012; 4:447-70; PMID:22590681; http://dx.doi.org/10.3390/v4040447
63. Dias JM, Kuehne AI, Abelson DM, Bale S, Wong AC, Halfmann P, Muhammad MA, Fusco ML, Zak SE, Kang E, et al. A shared structural solution for neutralizing ebolaviruses. Nat Struct Mol Biol 2011; 18:1424-7; PMID:22101933; http://dx.doi.org/10.1038/nsmb.2150
64. Binning JM, Wang T, Luthra P, Shabman RS, Borek DM, Liu G, Xu W, Leung DW, Basler CF, Amarasinghe GK. Development of RNA aptamers targeting Ebola virus VP35. Biochemistry 2013; 52:8406-19; PMID:24067086; http://dx.doi.org/10.1021/bi400704d
65. Malashkevich VN, Schneider BJ, McNally ML, Milhollen MA, Pang JX, Kim PS. Core structure of the envelope glycoprotein GP2 from Ebola virus at 1.9-A resolution. Proc Natl Acad Sci U S A 1999; 96:2662-7; PMID:10077567; http://dx.doi.org/10.1073/pnas.96.6.2662
66. Bornholdt ZA, Noda T, Abelson DM, Halfmann P, Wood MR, Kawaoka Y, Saphire EO. Structural rearrangement of ebola virus VP40 begets multiple functions in the virus life cycle. Cell 2013; 154:763-74; PMID:23953110; http://dx.doi.org/10.1016/j.cell.2013.07.015
67. Prins KC, Delpeut S, Leung DW, Reynard O, Volchkova VA, Reid SP, Ramanan P, Cardenas WB, Amarasinghe GK, Volchkov VE, et al. Mutations abrogating VP35 interaction with double-stranded RNA render Ebola virus avirulent in guinea pigs. J Virol 2010; 84:3004-15; PMID:20071589; http://dx.doi.org/10.1128/JVI.02459-09
68. Leung DW, Shabman RS, Farahbakhsh M, Prins KC, Borek DM, Wang T, Muhlberger E, Basler CF, Amarasinghe GK. Structural and functional characterization of Reston Ebola virus VP35 interferon inhibitory domain. J Mol Biol 2010; 399:347-57; PMID:20399790; http://dx.doi.org/10.1016/j.jmb.2010.04.022
69. Leung DW, Ginder ND, Fulton DB, Nix J, Basler CF, Honzatko RB, Amarasinghe GK. Structure of the Ebola VP35 interferon inhibitory domain. Proc Natl Acad Sci U S A 2009; 106:411-6;

PMID:19122151; http://dx.doi.org/10.1073/pnas.0807854106
70. Leung DW, Prins KC, Borek DM, Farahbakhsh M, Tufariello JM, Ramanan P, Nix JC, Helgeson LA, Otwinowski Z, Honzatko RB, et al. Structural basis for dsRNA recognition and interferon antagonism by Ebola VP35. Nat Struct Mol Biol 2010; 17:165-72; PMID:20081868; http://dx.doi.org/10.1038/nsmb.1765
71. Leung DW, Borek D, Luthra P, Binning JM, Anantpadma M, Liu G, Harvey IB, Su Z, Endlich-Frazier A, Pan J, et al. An Intrinsically Disordered Peptide from Ebola Virus VP35 Controls Viral RNA Synthesis by Modulating Nucleoprotein-RNA Interactions. Cell Rep 2015; 11:376-89; PMID:25865894; http://dx.doi.org/10.1016/j.celrep.2015.03.034
72. Modrof J, Becker S, Muhlberger E. Ebola virus transcription activator VP30 is a zinc-binding protein. J Virol 2003; 77:3334-8; PMID:12584359; http://dx.doi.org/10.1128/JVI.77.5.3334-3338.2003
73. Gough J, Karplus K, Hughey R, Chothia C. Assignment of homology to genome sequences using a library of hidden Markov models that represent all proteins of known structure. J Mol Biol 2001; 313:903-19; PMID:11697912; http://dx.doi.org/10.1006/jmbi.2001.5080
74. de Castro E, Sigrist CJ, Gattiker A, Bulliard V, Langendijk-Genevaux PS, Gasteiger E, Bairoch A, Hulo N. ScanProsite: detection of PROSITE signature matches and ProRule-associated functional and structural residues in proteins. Nucleic Acids Res 2006; 34:W362-5; PMID:16845026; http://dx.doi.org/10.1093/nar/gkl124
75. Tanner SJ, Ariza A, Richard CA, Kyle HF, Dods RL, Blondot ML, Wu W, Trincao J, Trinh CH, Hiscox JA, et al. Crystal structure of the essential transcription antiterminator M2-1 protein of human respiratory syncytial virus and implications of its phosphorylation. Proc Natl Acad Sci U S A 2014; 111:1580-5; PMID:24434552; http://dx.doi.org/10.1073/pnas.1317262111
76. Leyrat C, Renner M, Harlos K, Huiskonen JT, Grimes JM. Drastic changes in conformational dynamics of the antiterminator M2-1 regulate transcription efficiency in Pneumovirinae. eLife 2014; 3:e02674; PMID:24842877; http://dx.doi.org/10.7554/eLife.02674
77. Rudolph MG, Kraus I, Dickmanns A, Eickmann M, Garten W, Ficner R. Crystal structure of the borna disease virus nucleoprotein. Structure 2003; 11:1219-26; PMID:14527390; http://dx.doi.org/10.1016/j.str.2003.08.011
78. Green TJ, Zhang X, Wertz GW, Luo M. Structure of the vesicular stomatitis virus nucleoprotein-RNA complex. Science 2006; 313:357-60; PMID:16778022; http://dx.doi.org/10.1126/science.1126953
79. Albertini AA, Wernimont AK, Muziol T, Ravelli RB, Clapier CR, Schoehn G, Weissenhorn W, Ruigrok RW. Crystal structure of the rabies virus nucleoprotein-RNA complex. Science 2006; 313:360-3; PMID:16778023; http://dx.doi.org/10.1126/science.1125280
80. Tawar RG, Duquerroy S, Vonrhein C, Varela PF, Damier-Piolle L, Castagne N, MacLellan K, Bedouelle H, Bricogne G, Bhella D, et al. Crystal structure of a nucleocapsid-like nucleoprotein-RNA complex of respiratory syncytial virus. Science 2009; 326:1279-83; PMID:19965480; http://dx.doi.org/10.1126/science.1177634
81. Yabukarski F, Lawrence P, Tarbouriech N, Bourhis JM, Delaforge E, Jensen MR, Ruigrok RW, Blackledge M, Volchkov V, Jamin M. Structure of Nipah virus unassembled nucleoprotein in complex with its viral chaperone. Nat Struct Mol Biol 2014; 21:754-9; PMID:25108352; http://dx.doi.org/10.1038/nsmb.2868
82. Dong S, Yang P, Li G, Liu B, Wang W, Liu X, Xia B, Yang C, Lou Z, Guo Y, et al. Insight into the Ebola virus nucleocapsid assembly mechanism: crystal structure of Ebola virus nucleoprotein core domain at 1.8 A resolution. Protein cell 2015; 6:351-62; PMID:25910597; http://dx.doi.org/10.1007/s13238-015-0163-3
83. Gerlach P, Malet H, Cusack S, Reguera J. Structural Insights into Bunyavirus Replication and Its Regulation by the vRNA Promoter. Cell 2015; 161:1267-79; PMID:26004069; http://dx.doi.org/10.1016/j.cell.2015.05.006
84. Lu X, McDonald SM, Tortorici MA, Tao YJ, Vasquez-Del Carpio R, Nibert ML, Patton JT, Harrison SC. Mechanism for coordinated RNA packaging and genome replication by rotavirus polymerase VP1. Structure 2008; 16:1678-88; PMID:19000820; http://dx.doi.org/10.1016/j.str.2008.09.006
85. Tao Y, Farsetta DL, Nibert ML, Harrison SC. RNA synthesis in a cage–structural studies of reovirus polymerase lambda3. Cell 2002; 111:733-45; PMID:12464184; http://dx.doi.org/10.1016/S0092-8674(02)01110-8
86. Pan J, Vakharia VN, Tao YJ. The structure of a birnavirus polymerase reveals a distinct active site topology. Proc Natl Acad Sci U S A 2007; 104:7385-90; PMID:17456597; http://dx.doi.org/10.1073/pnas.0611599104
87. Bressanelli S, Tomei L, Rey FA, De Francesco R. Structural analysis of the hepatitis C virus RNA polymerase in complex with ribonucleotides. J Virol 2002; 76:3482-92; PMID:11884572; http://dx.doi.org/10.1128/JVI.76.7.3482-3492.2002
88. Ferrer-Orta C, Arias A, Perez-Luque R, Escarmis C, Domingo E, Verdaguer N. Structure of foot-and-mouth disease virus RNA-dependent RNA polymerase and its complex with a template-primer RNA. J Biol Chem 2004; 279:47212-21; PMID:15294895; http://dx.doi.org/10.1074/jbc.M405465200
89. te Velthuis AJ. Common and unique features of viral RNA-dependent polymerases. Cell Mol Life Sci 2014; 71:4403-20; PMID:25080879; http://dx.doi.org/10.1007/s00018-014-1695-z
90. Altschul SF, Madden TL, Schaffer AA, Zhang J, Zhang Z, Miller W, Lipman DJ. Gapped BLAST and PSI-BLAST: a new generation of protein database search programs. Nucleic Acids Res 1997; 25:3389-402; PMID:9254694; http://dx.doi.org/10.1093/nar/25.17.3389
91. Bouvet M, Ferron F, Imbert I, Gluais L, Selisko B, Coutard B, Canard B, Decroly E. [Capping strategies in RNA viruses]. Med Sci 2012; 28:423-9; PMID:22549871; http://dx.doi.org/10.1051/medsci/2012284021
92. Smietanski M, Werner M, Purta E, Kaminska KH, Stepinski J, Darzynkiewicz E, Nowotny M, Bujnicki JM. Structural analysis of human 2′-O-ribose methyltransferases involved in mRNA cap structure formation. Nat Commun 2014; 5:3004; PMID:24402442; http://dx.doi.org/10.1038/ncomms4004
93. Takada A, Fujioka K, Tsuiji M, Morikawa A, Higashi N, Ebihara H, Kobasa D, Feldmann H, Irimura T, Kawaoka Y. Human macrophage C-type lectin specific for galactose and N-acetylgalactosamine promotes filovirus entry. J Virol 2004; 78:2943-7; PMID:14990712; http://dx.doi.org/10.1128/JVI.78.6.2943-2947.2004
94. Yaddanapudi K, Palacios G, Towner JS, Chen I, Sariol CA, Nichol ST, Lipkin WI. Implication of a retrovirus-like glycoprotein peptide in the immunopathogenesis of Ebola and Marburg viruses. FASEB J 2006; 20:2519-30; PMID:17023517; http://dx.doi.org/10.1096/fj.06-6151com
95. Kash JC, Muhlberger E, Carter V, Grosch M, Perwitasari O, Proll SC, Thomas MJ, Weber F, Klenk HD, Katze MG. Global suppression of the host antiviral response by Ebola- and Marburgviruses: increased antagonism of the type I interferon response is associated with enhanced virulence. J Virol 2006; 80:3009-20; PMID:16501110; http://dx.doi.org/10.1128/JVI.80.6.3009-3020.2006
96. Cardenas WB, Loo YM, Gale M Jr., Hartman AL, Kimberlin CR, Martinez-Sobrido L, Saphire EO, Basler CF. Ebola virus VP35 protein binds double-stranded RNA and inhibits α/β interferon production induced by RIG-I signaling. J Virol 2006; 80:5168-78; PMID:16698997; http://dx.doi.org/10.1128/JVI.02199-05
97. Volchkov VE, Chepurnov AA, Volchkova VA, Ternovoj VA, Klenk HD. Molecular characterization of guinea pig-adapted variants of Ebola virus. Virol 2000; 277:147-55; PMID:11062045; http://dx.doi.org/10.1006/viro.2000.0572
98. Ebihara H, Takada A, Kobasa D, Jones S, Neumann G, Theriault S, Bray M, Feldmann H, Kawaoka Y. Molecular determinants of Ebola virus virulence in mice. PLoS Pathog 2006; 2:e73; http://dx.doi.org/10.1371/journal.ppat.0020073
99. Kondratowicz AS, Lennemann NJ, Sinn PL, Davey RA, Hunt CL, Moller-Tank S, Meyerholz DK, Rennert P, Mullins RF, Brindley M, et al. T-cell immunoglobulin and mucin domain 1 (TIM-1) is a receptor for Zaire Ebolavirus and Lake Victoria Marburgvirus. Proc Natl Acad Sci U S A 2011; 108:8426-31; PMID:21536871; http://dx.doi.org/10.1073/pnas.1019030108
100. Alvarez CP, Lasala F, Carrillo J, Muniz O, Corbi AL, Delgado R. C-type lectins DC-SIGN and L-SIGN mediate cellular entry by Ebola virus in cis and in trans. J Virol 2002; 76:6841-4; PMID:12050398; http://dx.doi.org/10.1128/JVI.76.13.6841-6844.2002
101. Simmons G, Reeves JD, Grogan CC, Vandenberghe LH, Baribaud F, Whitbeck JC, Burke E, Buchmeier MJ, Soilleux EJ, Riley JL, et al. DC-SIGN and DC-SIGNR bind ebola glycoproteins and enhance infection of macrophages and endothelial cells. Virol 2003; 305:115-23; PMID:12504546; http://dx.doi.org/10.1006/viro.2002.1730
102. Chan SY, Empig CJ, Welte FJ, Speck RF, Schmaljohn A, Kreisberg JF, Goldsmith MA. Folate receptor-α is a cofactor for cellular entry by Marburg and Ebola viruses. Cell 2001; 106:117-26; PMID:11461707; http://dx.doi.org/10.1016/S0092-8674(01)00418-4
103. Chandran K, Sullivan NJ, Felbor U, Whelan SP, Cunningham JM. Endosomal proteolysis of the Ebola virus glycoprotein is necessary for infection. Science 2005; 308:1643-5; PMID:15831716; http://dx.doi.org/10.1126/science.1110656
104. Sullivan NJ, Peterson M, Yang ZY, Kong WP, Duckers H, Nabel E, Nabel GJ. Ebola virus glycoprotein toxicity is mediated by a dynamin-dependent protein-trafficking pathway. J Virol 2005; 79:547-53; PMID:15596847; http://dx.doi.org/10.1128/JVI.79.1.547-553.2005
105. Halfmann P, Neumann G, Kawaoka Y. The Ebolavirus VP24 protein blocks phosphorylation of p38 mitogen-activated protein kinase. J Infect Dis 2011; 204 Suppl 3:S953-6; PMID:21987775; http://dx.doi.org/10.1093/infdis/jir325
106. Fabozzi G, Nabel CS, Dolan MA, Sullivan NJ. Ebolavirus proteins suppress the effects of small interfering RNA by direct interaction with the mammalian RNA interference pathway. J Virol 2011; 85:2512-23; PMID:21228243; http://dx.doi.org/10.1128/JVI.01160-10
107. Shabman RS, Leung DW, Johnson J, Glennon N, Gulcicek EE, Stone KL, Leung L, Hensley L, Amarasinghe GK, Basler CF. DRBP76 associates with Ebola virus VP35 and suppresses viral polymerase function. J Infect Dis 2011; 204 Suppl 3:S911-8; PMID:21987769; http://dx.doi.org/10.1093/infdis/jir343
108. Prins KC, Cardenas WB, Basler CF. Ebola virus protein VP35 impairs the function of interferon regulatory factor-activating kinases IKKepsilon and TBK-1.

J Virol 2009; 83:3069-77; PMID:19153231; http://dx.doi.org/10.1128/JVI.01875-08
109. Luthra P, Ramanan P, Mire CE, Weisend C, Tsuda Y, Yen B, Liu G, Leung DW, Geisbert TW, Ebihara H, et al. Mutual antagonism between the Ebola virus VP35 protein and the RIG-I activator PACT determines infection outcome. Cell Host Microbe 2013; 14:74-84; PMID:23870315; http://dx.doi.org/10.1016/j.chom.2013.06.010
110. Feng Z, Cerveny M, Yan Z, He B. The VP35 protein of Ebola virus inhibits the antiviral effect mediated by double-stranded RNA-dependent protein kinase PKR. J Virol 2007; 81:182-92; PMID:17065211; http://dx.doi.org/10.1128/JVI.01006-06
111. Chang TH, Kubota T, Matsuoka M, Jones S, Bradfute SB, Bray M, Ozato K. Ebola Zaire virus blocks type I interferon production by exploiting the host SUMO modification machinery. PLoS Pathog 2009; 5:e1000493; PMID:19557165; http://dx.doi.org/10.1371/journal.ppat.1000493
112. Kubota T, Matsuoka M, Chang TH, Bray M, Jones S, Tashiro M, Kato A, Ozato K. Ebolavirus VP35 interacts with the cytoplasmic dynein light chain 8. J Virol 2009; 83:6952-6; PMID:19403681; http://dx.doi.org/10.1128/JVI.00480-09
113. Yamayoshi S, Noda T, Ebihara H, Goto H, Morikawa Y, Lukashevich IS, Neumann G, Feldmann H, Kawaoka Y. Ebola virus matrix protein VP40 uses the COPII transport system for its intracellular transport. Cell Host Microbe 2008; 3:168-77; PMID:18329616; http://dx.doi.org/10.1016/j.chom.2008.02.001
114. Garcia M, Cooper A, Shi W, Bornmann W, Carrion R, Kalman D, Nabel GJ. Productive replication of Ebola virus is regulated by the c-Abl1 tyrosine kinase. Sci Transl Med 2012; 4:123ra124; http://dx.doi.org/10.1126/scitranslmed.3003500
115. Harty RN, Brown ME, Wang G, Huibregtse J, Hayes FP. A PPxY motif within the VP40 protein of Ebola virus interacts physically and functionally with a ubiquitin ligase: implications for filovirus budding. Proc Natl Acad Sci U S A 2000; 97:13871-6; PMID:11095724; http://dx.doi.org/10.1073/pnas.250277297
116. Ruthel G, Demmin GL, Kallstrom G, Javid MP, Badie SS, Will AB, Nelle T, Schokman R, Nguyen TL, Carra JH, et al. Association of ebola virus matrix protein VP40 with microtubules. J Virol 2005; 79:4709-19; PMID:15795257; http://dx.doi.org/10.1128/JVI.79.8.4709-4719.2005
117. Han Z, Harty RN. Packaging of actin into Ebola virus VLPs. Virol J 2005; 2:92; PMID:16367999; http://dx.doi.org/10.1186/1743-422X-2-92
118. Lu J, Qu Y, Liu Y, Jambusaria R, Han Z, Ruthel G, Freedman BD, Harty RN. Host IQGAP1 and Ebola virus VP40 interactions facilitate virus-like particle egress. J Virol 2013; 87:7777-80; PMID:23637409; http://dx.doi.org/10.1128/JVI.00470-13
119. Jeffers SA, Sanders DA, Sanchez A. Covalent modifications of the ebola virus glycoprotein. J Virol 2002; 76:12463-72; PMID:12438572; http://dx.doi.org/10.1128/JVI.76.24.12463-12472.2002
120. Manicassamy B, Wang J, Jiang H, Rong L. Comprehensive analysis of ebola virus GP1 in viral entry. J Virol 2005; 79:4793-805; PMID:15795265; http://dx.doi.org/10.1128/JVI.79.8.4793-4805.2005
121. Haasnoot J, de Vries W, Geutjes EJ, Prins M, de Haan P, Berkhout B. The Ebola virus VP35 protein is a suppressor of RNA silencing. PLoS Pathog 2007; 3:e86; PMID:17590081; http://dx.doi.org/10.1371/journal.ppat.0030086
122. Schumann M, Gantke T, Muhlberger E. Ebola virus VP35 antagonizes PKR activity through its C-terminal interferon inhibitory domain. J Virol 2009; 83:8993-7; PMID:19515768; http://dx.doi.org/10.1128/JVI.00523-09
123. McCarthy SE, Johnson RF, Zhang YA, Sunyer JO, Harty RN. Role for amino acids 212KLR214 of Ebola virus VP40 in assembly and budding. J Virol 2007; 81:11452-60; PMID:17699576; http://dx.doi.org/10.1128/JVI.00853-07
124. Yamayoshi S, Kawaoka Y. Mapping of a region of Ebola virus VP40 that is important in the production of virus-like particles. J Infect Dis 2007; 196 Suppl 2:S291-5; PMID:17940963; http://dx.doi.org/10.1086/520595
125. Adu-Gyamfi E, Soni SP, Jee CS, Digman MA, Gratton E, Stahelin RV. A loop region in the N-terminal domain of Ebola virus VP40 is important in viral assembly, budding, and egress. Viruses 2014; 6:3837-54; PMID:25330123; http://dx.doi.org/10.3390/v6103837
126. Adu-Gyamfi E, Soni SP, Xue Y, Digman MA, Gratton E, Stahelin RV. The Ebola virus matrix protein penetrates into the plasma membrane: a key step in viral protein 40 (VP40) oligomerization and viral egress. J Biol Chem 2013; 288:5779-89; PMID:23297401; http://dx.doi.org/10.1074/jbc.M112.443960